Central finite volume methods with constrained transport divergence treatment for ideal MHD

P. Arminjon [a,*], R. Touma [b]

[a] *Centre de Recherches Mathématiques, Université de Montréal, C.P. 6128, Succ. Centre-ville, Montreal, Que., Canada H3C 3J7*
[b] *Département de Mathématiques et de Statistique, Université de Montréal, Canada*

Abstract

Two and three-dimensional finite volume extensions of the Lax–Friedrichs (LF) and Nessyahu–Tadmor one-dimensional difference schemes were previously presented and successfully applied to several problems for nonlinear hyperbolic systems, and in particular to typical test cases for both inviscid and viscous compressible flows. These ''central'' schemes by-pass the resolution, at the cell interfaces, of the Riemann problems, thanks to the use of the staggered LF scheme which serves as the base scheme on which high order finite volume methods can be constructed using van Leer's MUSCL-type limited reconstruction principle. For this purpose, two dual grids are used at alternate time steps. These methods are extended here to several problems in one- and multi-dimensional ideal compressible magnetohydrodynamics using a modified version of the first author's central methods with oblique (diamond shaped) dual cells. In two-dimensions the system has eight equations and solving the corresponding Riemann problem is an elaborate and time-consuming process. Central methods lead to significant computing time reductions, and the numerical experiments presented here suggest the accuracy is quite satisfactory. In order to satisfy the physical constraint $\nabla \cdot \mathbf{B} = 0$, we have constructed a strategy (''CTCS'') inspired from the *Constrained Transport* method of Evans and Hawley. The validity of our base scheme and our CTCS approach is clearly confirmed by the results.
© 2004 Elsevier Inc. All rights reserved.

Keywords: Numerical methods; Magnetohydrodynamics; Central schemes; Non-oscillatory

---

* Corresponding author.
 E-mail addresses: arminjon@crm.umontreal.ca (P. Arminjon), touma@dms.umontreal.ca (R. Touma).

1. Introduction

1.1. Some previous work on multi-dimensional central schemes

Many problems in applied mathematics, physics and the engineering sciences can be formulated mathematically with the help of an idealized model based on hyperbolic partial differential equations and more specifically hyperbolic systems of conservation laws [22] or, in the case of systems with a source term, hyperbolic systems of balance laws [43]. In the past thirty years or so, and following the first fundamental papers of Godunov [23], Lax and Wendroff [34], an enormous amount of work has appeared on the subject of numerical methods for these problems and in particular for the development of non-oscillatory, high-order "shock-capturing" methods for conservation laws and their many applications, particularly for compressible flows and aerodynamics [26]; see the expository works [24,47,25,22,31,35,46,42]. We apologize in advance to the many important contributors whose name could not be explicitly mentioned in this paper. With the appearance of finite volume methods, based on Godunov's principle of integrating the PDE on the discrete cells [23], and upwind methods including Godunov's method, as well as the methods of Murman–Cole [25], Steger–Warming [25], users had the choice between many options and in particular between upwind schemes, including those based on Riemann's solvers, and centered schemes with the addition of some kind of artificial viscosity to stabilize the scheme and avoid oscillations near discontinuities [26].

In another approach the Nessyahu–Tadmor one-dimensional finite difference scheme ("NT") [37] led to the additional option of a Godunov-type scheme without the requirement to solve the Riemann problems at the cell interfaces, thanks to the use of a staggered form of the Lax–Friedrichs scheme as a base scheme, complemented by van Leer's "MUSCL"-type limited reconstructions for higher accuracy [50,51]. This scheme, which uses two alternate, dual grids at alternate time steps, was recently extended to multi-dimensional finite volume versions for Cartesian grids [2,28] as well as unstructured triangular [1,3] and tetrahedral grids [7,10]. More recently, we constructed [9] modified versions of the above schemes which avoid the time predictor step typical of the original NT scheme formulation, and therefore lead to time reductions of about 40%.

Another approach to improve these schemes consists in applying Runge–Kutta methods for the integration with respect to time [38] where so-called "central Runge–Kutta schemes" have been proposed and successfully tested. In the case of Cartesian grids, we also presented [6,8,10,11] a modified scheme introducing new oblique dual cells ("diamond cells") instead of the dual cells with sides parallel to the coordinates axes originally considered in [2] for the second grid. These diamond cells were in fact the direct analogue of the quadrilateral dual cells introduced in the two-dimensional finite volume extension of the NT scheme described in [1,3] for unstructured triangular grids. They have also been considered, independently, by Katsaounis and Levy [30]; combined with the use of standard limiters, they lead to second-order accuracy and monotonicity preservation, in the case of continuous initial data.

They often lead to better L^1 and L^∞ errors, improved resolution of oblique shocks, and to higher orders of accuracy (see [8]). They also tend to prevent the crossing of discontinuities in the normal direction.

Instead of modifying the dual cells to improve the accuracy, another approach consisting of modifying the numerical flux by using an improved quadrature formula for the fluxes across the cell boundaries has recently been proposed by Lie and Noelle [36]. Their scheme is less sensitive to grid orientation effects and leads to an improved preservation of symmetries as compared with the original two-dimensional finite volume extensions of the NT scheme considered in [8].

1.2. Previous work on numerical MHD

The adaptation of shock capturing numerical methods to the equations of Magnetohydrodynamics (MHD) has been a very dynamic and continuous process since the early eighties; without attempting to

be complete, let us mention the early work of Brackbill and Barnes [15], who proposed a "projection scheme" to satisfy the div $\vec{\mathbf{B}} = 0$ constraint, involving the solution of a Poisson equation. Since Magneto-hydrodynamics plays an important role in astrophysical flows, which are highly compressible, it was soon observed that Godunov-type methods might be a useful approach to solve these problems: Brio and Wu [16] applied Roe's method to the one-dimensional MHD equations. Zachary and Colella [52] used the Engquist–Osher flux solver for one-dimensional ideal MHD, which was then extended to multi-dimensional ideal MHD in Zachary et al. [53].

Dai and Woodward [17] presented a nonlinear approximate Riemann solver specifically designed for MHD problems, and extended the piecewise parabolic method to multi-dimensional MHD problems [19]. They also made important contributions in [18] with a second-order accurate difference scheme for multi-dimensional MHD using an approximate MHD Riemann solver, and an approach to maintain the divergence-free condition exactly.

Powell [41] and Powell et al. [40,39] developed a Roe-type Riemann solver and, using a non-conservative form of the MHD equations, an upwind scheme for MHD equations, the "8-wave Riemann solver method" (where the eighth wave is associated with propagation of div $\vec{\mathbf{B}}$) which proved to be numerically robust. Finally, Ryu and Jones [44], Barmin et al. [14] Tóth and Odstrčil [49] Balsara [13] all applied TVD-type methods to the MHD equations.

1.3. Contents of the paper

In this paper we extend central NT-type one-dimensional or multi-dimensional finite volume schemes to the resolution of some problems in ideal (inviscid and non-resistive) compressible MHD. The system of governing equations features eight nonlinear hyperbolic conservation equations for mass, linear momentum, energy and the three components of the magnetic field vector $\vec{\mathbf{B}}$. Even in the case where $\vec{\mathbf{B}}$ only depends on one space variable, the system still has eight equations but can be reduced to seven equations thanks to the physical constraint $\nabla \cdot \mathbf{B} = 0$. The subject of how one should best try to satisfy this constraint for multi-dimensional problems has been discussed in several important papers [48,15,39,41,40,17–19].

The Jacobian matrix in this case is thus a 7×7 matrix of which 5 of the 7 eigenvalues may coincide [16]. Moreover, the system of MHD equations is nonconvex [20]. This gives rise to a wave structure which is substantially more complicated than that of the Euler equations for compressible flow. In particular so-called compound waves may appear, which consist of a shock and, directly attached, a rarefaction wave. The solution of the corresponding Riemann problem, exact or approximate, is a complicated and time-consuming process. We expect the introduction of our Riemann solver-free central methods to lead to significant computing time reductions in two or three space dimensions.

 (i) In one-dimension, we present an adaptation of the NT scheme to two variants of the MHD-shock tube problem [16] which leads to fairly good results, and, compared with a method based on Riemann solvers, is also likely to bring about significant computing time reductions, as was the case for the Euler and Navier–Stokes equations [2–4].
(ii) We also studied, in two spatial dimensions, the 2D Riemann problem with continuation boundary conditions originally considered without the magnetic field by [45] and later, in an MHD context, by Dai–Woodward [18]. We then solve the Orszag–Tang MHD turbulence problem which describes the evolution of a compressible vortex system. The problem involves the interaction between several shock waves traveling at various speed regimes. We apply our new Constrained Transport method to numerically enforce the physical constraint on the magnetic field.

The organization of the paper is as follows. In Section 2 we describe the mathematical formulation of multi-dimensional MHD problems. Section 3 presents a short review of the one-dimensional NT finite

difference scheme. Section 4 gives a complete description of our two-dimensional finite volume extension of the NT scheme using diamond staggered dual cells. In section 5 we present the physical constraint on the magnetic field and describe several methods to satisfy the divergence-free property of the magnetic field. We then introduce our method for enforcing the $\nabla \cdot \mathbf{B} = 0$ constraint. One and two-dimensional numerical results are presented in section 6.

2. Ideal MHD equations

When a conducting fluid moves in a magnetic field, electric fields are induced in it and electric currents flow. Due to the magnetic field, the currents may modify the flow. Conversely, the currents themselves modify the magnetic field [27], and even if the components of $\mathbf{B}$ only depend on one variable, say x, the magnetic forces exerted on the ions constituting the "plasma", i.e., the fluid (gas) in motion are three-dimensional, thus giving rise to a three-dimensional flow. The complex interaction between magnetic and fluid dynamic phenomena is well described by a set of eight equations which are: one mass conservation law, three momentum conservation laws, one energy conservation law and Faraday's (three-dimensional) law for the magnetic field $\mathbf{B}$:

$$\frac{\partial}{\partial t} \begin{bmatrix} \rho \\ \rho\mathbf{u} \\ \rho e \\ \mathbf{B} \end{bmatrix} + \nabla \cdot \begin{bmatrix} \rho\mathbf{u} \\ \rho\mathbf{u}\mathbf{u} + I(p + \frac{\mathbf{B}\cdot\mathbf{B}}{2\mu_0}) - \frac{\mathbf{B}\mathbf{B}}{\mu_0} \\ (\rho e + p + \frac{\mathbf{B}\cdot\mathbf{B}}{2\mu_0})\mathbf{u} - \frac{1}{\mu_0}(\mathbf{u}\cdot\mathbf{B})\mathbf{B} \\ \mathbf{u}\mathbf{B} - \mathbf{B}\mathbf{u} \end{bmatrix} = 0, \tag{1}$$

where ρ, $\mathbf{u}$, p, $\mathbf{B}$ and e are the mass density, three-component velocity field vector, thermal pressure, three-component magnetic field vector and the specific total energy; μ_0 is the permeability of the vacuum and I is the (3×3) identity matrix. This system of equations is completed by the equation of state $p = (\gamma - 1)\rho\epsilon$, where γ is the ratio of specific heats and ϵ denotes the specific internal energy. It is usual to non-dimensionalize the ideal MHD equations, by setting reference scales for the length L or the free-stream density ρ_∞, and scaling the current magnetic field with $\sqrt{\mu_0}$, which results in the removal of μ_0 from the above system. In this paper, no scaling is applied so the permeability term of the vacuum is kept.

The two-dimensional version of the system takes the following form:

$$\frac{\partial \overrightarrow{U}}{\partial t} + \frac{\partial \overrightarrow{F}}{\partial x} + \frac{\partial \overrightarrow{G}}{\partial y} = 0, \tag{2}$$

with

$$\overrightarrow{U} = \begin{pmatrix} \rho \\ \rho u_x \\ \rho u_y \\ \rho u_z \\ \rho e \\ B_x \\ B_y \\ B_z \end{pmatrix}, \quad \overrightarrow{F}(\overrightarrow{U}) = \begin{pmatrix} \rho u_x \\ \rho u_x^2 + \Pi_{xx} \\ \rho u_x u_y + \Pi_{xy} \\ \rho u_x u_z + \Pi_{xz} \\ \rho u_x e + u_x \Pi_{xx} + u_y \Pi_{xy} + u_z \Pi_{xz} \\ 0 \\ \Lambda_z \\ -\Lambda_y \end{pmatrix}, \quad \overrightarrow{G}(\overrightarrow{U}) = \begin{pmatrix} \rho u_y \\ \rho u_y u_x + \Pi_{xy} \\ \rho u_y^2 + \Pi_{yy} \\ \rho u_y u_z + \Pi_{yz} \\ \rho u_y e + u_x \Pi_{xy} + u_y \Pi_{yy} + u_z \Pi_{yz} \\ -\Lambda_z \\ 0 \\ \Lambda_x \end{pmatrix}, \tag{3}$$

where $\Lambda \equiv \mathbf{u} \times \mathbf{B}$, e is the specific total energy, Π_{xx}, Π_{yy} and Π_{zz} are the diagonal elements of the total pressure tensor, Π_{xy}, Π_{xz} and Π_{yz} are the off-diagonal elements of the tensor which may be obtained from system (1)

$$\Pi_{ii} = p + \frac{1}{8\pi}\left(B_j^2 + B_k^2 - B_i^2\right),$$

$$\Pi_{ij} = -\frac{1}{4\pi}B_i B_j, \quad \text{for } i,j,k = x,y,z,$$

$$e = \epsilon + \frac{1}{2}\mathbf{u}^2 \frac{1}{8\pi\rho}\mathbf{B}^2.$$

In the case of one-dimensional MHD, the divergence-free constraint reduces the differential system (2) to the form $\overrightarrow{U}_t + \overrightarrow{F}_x = 0$ with seven equations by freezing the value of the x-component of the magnetic field, giving rise to the vectors $\overrightarrow{U} = (\rho, \rho u_x, \rho u_y, \rho u_z, \rho e, B_y, B_z)$ and $\overrightarrow{F} = (\rho u_x, \rho u_x^2 + \Pi_{xx}, \rho u_x u_y + \Pi_{xy}, \rho u_x u_z + \Pi_{xz}, \rho u_x e + u_x \Pi_{xx} + u_y \Pi_{xy} + u_z \Pi_{xz}, \Lambda_z, -\Lambda_y)$. The resulting system allows three kinds of waves [32,27,18,20]: fast waves, Alfven waves and slow waves. These waves have propagation speeds denoted respectively by C_f, C_a and C_s which are the eigenvalues of the differential system, given by

$$C_{f,s}^2 = \frac{1}{2}\left[(C_o^2 + C_a^2 + C_t^2) \pm \sqrt{(C_o^2 + C_a^2 + C_t^2)^2 - 4C_o^2 C_a^2}\right], \tag{4}$$

$$C_a = \sqrt{\rho B_x^2/(4\pi)} \tag{5}$$

with $C_o = \sqrt{\gamma p/\rho}$, $C_t = \sqrt{\rho(B_y^2 + B_z^2)/(4\pi)}$. For a complete presentation of the eigensystem, the interested reader is referred to [27,32]. We recall that eigenvalues are used in the CFL condition to determine the time step.

3. One-dimensional central schemes

We consider the initial value problem

$$u_t + f(u)_x = 0,$$
$$u(x, t = 0) = u_o(x) \tag{6}$$

and the (first-order accurate) Lax–Friedrichs scheme [33] written in its staggered form as

$$u_{i+1/2}^{n+1} = \frac{1}{2}(u_{i+1}^n + u_i^n) - \lambda(f(u_{i+1}^n) - f(u_i^n)). \tag{7}$$

To obtain a second-order accurate scheme, Nessyahu and Tadmor's [37] introduced van Leer's MUSCL-type [50] piecewise linear reconstruction of the piecewise constant solution obtained at the previous step (i.e., at time t^n) (see Fig. 1)

$$u(x, t^n) = L_i(x, t^n) = u_i^n + (x - x_i)\frac{u_i'}{\Delta x}, \quad x \in [x_{i-1/2}, x_{i+1/2}], \tag{8}$$

where

$$u_i' = (u_i^n)' \cong h\frac{\partial}{\partial x}u(x, t^n)|_{x=x_i} + \mathrm{O}(\Delta x^2), \tag{9}$$
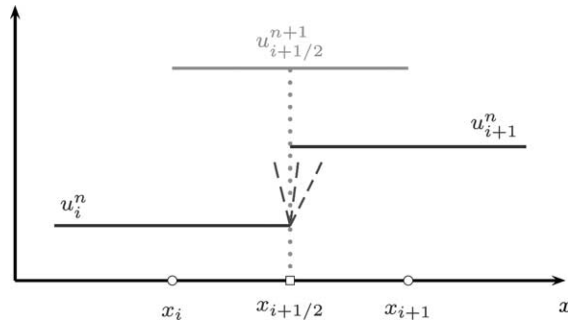
Fig. 1. The resolution of Riemann problems at cell interfaces is avoided when alternating from original to staggered grid.

approximates the slope to first-order accuracy; this leads to second-order spatial accuracy. Second-order accuracy with respect to time is then obtained if we apply the midpoint rule for the time integral of the flux [37]. Nessyahu and Tadmor's formula [37] gives the solution on the staggered grid (i.e., at nodes $x_{i+1/2}$)

$$u_{i+1/2}^{n+1} = \frac{1}{2}(u_{i+1}^n + u_i^n) + \frac{1}{8}((u_i^n)' - (u_{i+1}^n)') - \lambda(f(u_{i+1}^{n+1/2}) - f(u_i^{n+1/2})), \qquad (10)$$

where $u_i^{n+1/2}$ is an approximate value defined by an intermediate predictor step at time $t^{n+1/2}$. The solution at the nodes of the original grid $\{x_i\}$ and time t^{n+2} is obtained in a similar way.

4. Two-dimensional Cartesian diamond-staggered scheme

We consider a two-dimensional hyperbolic system of conservation laws

$$\overrightarrow{U}_t + \nabla \cdot \overrightarrow{F}(\overrightarrow{U}) \equiv \overrightarrow{U}_t + \overrightarrow{f}_x + \overrightarrow{g}_y = 0, \qquad (11)$$

where

$$\overrightarrow{U} = \begin{pmatrix} u_1 \\ u_2 \\ \vdots \\ u_n \end{pmatrix}, \quad \overrightarrow{F}(\overrightarrow{U}) = (\overrightarrow{f}, \overrightarrow{g}); \qquad \overrightarrow{f} = \begin{pmatrix} f_1 \\ f_2 \\ \vdots \\ f_n \end{pmatrix}, \quad \overrightarrow{g} = \begin{pmatrix} g_1 \\ g_2 \\ \vdots \\ g_n \end{pmatrix},$$

with the initial condition $\overrightarrow{U}(x, y, 0) = \overrightarrow{U}_o(x, y)$. System (11) is assumed to be hyperbolic in the sense that any linear combination of the $n \times n$ Jacobian matrices $A(\overrightarrow{U})$, $B(\overrightarrow{U})$

$$A(\overrightarrow{U}) = \frac{\partial \overrightarrow{f}}{\partial \overrightarrow{U}}, \quad B(\overrightarrow{U}) = \frac{\partial \overrightarrow{g}}{\partial \overrightarrow{U}}$$

has n real eigenvalues and n linearly independent right and left eigenvectors. As is well known, both the one-dimensional Lax–Friedrichs and Nessyahu–Tadmor schemes use alternate space grids. In two-dimensions, we shall proceed in a similar manner starting from the original Cartesian grid with cells C_i at time t^n, alternating to the diamond dual cell $D_{i+1/2,j}$ at time t^{n+1}, and returning back to the original cell C_i of the original structured grid as shown in Figs. 2 and 6.

Notations. We consider for our computational domain a uniform rectangular grid with M^2 squares; the extension to arbitrary rectangular grids is straightforward, except for the initialization, which requires

numerical integration, and for the programming part of the resolution, where we have to proceed as in the case of a fully unstructured grid. Let $\Delta x = \Delta y = h = x_{i+1/2} - x_{i-1/2}$ denote the mesh size, $a_{i,j} = (x_i, y_j) = (ih, jh)$, $0 \leqslant i, j \leqslant M$, denote the nodes of the first grid. For any arbitrary node $a_{i,j}$ we consider the corresponding finite volume cell $C_{i,j}$ for the first grid to be the square centered at $a_{i,j}$ with edges obtained by joining the centroids of the four squares of the original grid adjacent to $a_{i,j}$ as in Fig. 2.

The diamond dual cells $D_{i+1/2,j}$ are obtained by first considering two successive nodes $a_{i,j}$ and $a_{i+1,j}$ of the original grid; let $[TB]$ denote the common interface of the Cartesian cells; the midpoint of $[TB]$ is m. As can be seen from Fig. 2 there are two cases for the dual diamond cells, depending on whether the axis joining the two nodes of the original grid used to define the diamond cell is parallel to the x-axis or the y-axis. The dual cell (in the x-direction) is defined to be the quadrilateral $a_{i,j}Ta_{i,j+1}B$ as in Fig. 3. The dual cell $D_{i,j+1/2}$ is obtained when the edge $a_{i,j}a_{i,j+1}$ is parallel to the y-axis.

Let $\overrightarrow{U}_{i,j}^n \cong \overrightarrow{U}(a_{i,j}, t^n)$ and $\overrightarrow{U}_{i+1/2,j}^{n+1} \cong \overrightarrow{U}(m, t^{n+1})$ denote the average values in the first and second grid at time t^n and t^{n+1}, respectively. Performing the first time step gives $\overrightarrow{U}_{i+1/2,j}^{n+1}$ while the cell values $\{\overrightarrow{U}_{i,j}^{n+2}\}$ are obtained at the end of the second time-step.

4.1. First time step, in the x-direction

We consider here two adjacent nodes $a_{i,j}$ and $a_{i+1,j}$, where $a_{i,j}a_{i+1,j}$ is parallel to the x-axis, and $D_{i+1/2,j}$ denotes the corresponding dual cell (Fig. 3). We integrate Eq. (11) on $D_{i+1/2,j} \times [t^n, t^{n+1}]$

$$\int_{t^n}^{t^{n+1}} \int \int_{D_{i+1/2,j}} \overrightarrow{U}_t \, dA \, dt = -\int_{t^n}^{t^{n+1}} \int \int_{D_{i+1/2,j}} \nabla \cdot \overrightarrow{F} \, dA \, dt. \tag{12}$$
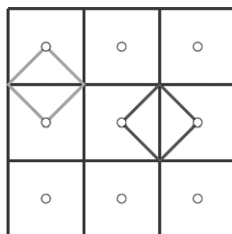
Applying Green's theorem gives

Fig. 2. Original data grid 'o', square cells in blue and two dual oblique cells in red. (For interpretation of the references to color in this figure legend, the reader is referred to the web version of this article.)
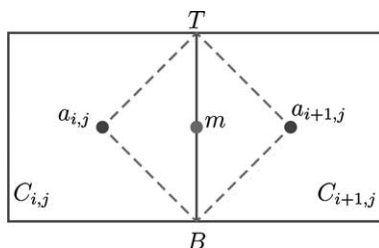

Fig. 3. Dual oblique cell $D_{i+1/2,j}$; case when the line through the centroids of the adjacent Cartesian cells is parallel to the x-axis.

$$\int\int_{D_{i+1/2,j}} \overrightarrow{U}(x,y,t^{n+1})\,\mathrm{d}A = \int\int_{D_{i+1/2,j}} \overrightarrow{U}(x,y,t^n)\,\mathrm{d}A - \int_{t^n}^{t^{n+1}} \oint_{\partial D_{i+1/2,j}} (\overrightarrow{f}\,n_x + \overrightarrow{g}\,n_y)\,\mathrm{d}\sigma\,\mathrm{d}t, \tag{13}$$

where $\overrightarrow{n} = (n_x, n_y)$ is the unit outward normal vector to the boundary of the diamond cell $\partial D_{i+1/2,j}$. The left-hand side of Eq. (13) defines the average value $\overrightarrow{U}_{i+1/2,j}^{n+1}$

$$\mathscr{A}(D_{i+1/2,j})\overrightarrow{U}_{i+1/2,j}^{n+1} \approx \int\int_{D_{i+1/2,j}} \overrightarrow{U}(x,y,t^{n+1})\,\mathrm{d}A, \tag{14}$$

where $\mathscr{A}(D_{i+1/2,j})$ denotes the area of the dual cell. We split the first integral of the right-hand side of Eq. (13) into two integrals

$$\int\int_{D_{i+1/2,j}} \overrightarrow{U}(x,y,t^n)\,\mathrm{d}A = \int\int_{D_{i+1/2,j}\cap C_{i,j}} \overrightarrow{U}(x,y,t^n)\,\mathrm{d}A + \int\int_{D_{i+1/2,j}\cap C_{i+1,j}} \overrightarrow{U}(x,y,t^n)\,\mathrm{d}A, \tag{15}$$

where $D_{i+1/2,j} \cap C_{i,j}$ is the triangle $a_{i,j}TB$, $D_{i+1/2,j} \cap C_{i+1,j}$ is the triangle $a_{i+1,j}TB$.

Eq. (15) is approximated to second-order [5] accuracy by

$$\int\int_{D_{i+1/2,j}} \overrightarrow{U}(x,y,t^n)\,\mathrm{d}A \cong \overrightarrow{U}\left(x_i + \frac{\Delta x}{3}, y_i, t^n\right)A(D_{i+1/2,j}\cap C_{i,j}) + \overrightarrow{U}\left(x_{i+1} - \frac{\Delta x}{3}, y_j, t^n\right)A(D_{i+1/2,j}$$
$$\cap C_{i+1,j}). \tag{16}$$

The term $\mathscr{A}(D_{i+1/2,j} \cap C_{i,j}) = h^2/4$ is the area of the triangle $a_{i,j}TB$.

Applying van Leer's (MUSCL) [50] piecewise linear interpolants defined at a node $a_{i,j}$ by

$$\widetilde{\overrightarrow{U}}_{i,j}(x,y,t^n) \cong \overrightarrow{U}_{i,j}^n + \frac{x-x_i}{\Delta x}\overrightarrow{U}_{i,j;x}^{\lim} + \frac{y-y_j}{\Delta y}\overrightarrow{U}_{i,j;y}^{\lim} \tag{17}$$

will guarantee second-order accuracy and preserve the monotonicity. Here $(\nabla\overrightarrow{U})^{\lim} \equiv (\overrightarrow{U}_x^{\lim}/\Delta x, \overrightarrow{U}_y^{\lim}/\Delta y)$ is a limited numerical gradient. Using Eqs. (16) and (17) we obtain

$$\int\int_{D_{i+1/2,j}} \overrightarrow{U}(x,y,t^n)\,\mathrm{d}A \cong \frac{h^2}{4}\left(\overrightarrow{U}_{i,j}^n + \overrightarrow{U}_{i+1,j}^n + \frac{1}{3}\overrightarrow{U}_{i,j;x}^{\lim} - \frac{1}{3}\overrightarrow{U}_{i+1,j;x}^{\lim}\right). \tag{18}$$

The integration of the flux-integral with respect to time is approximated to second-order accuracy with the help of the midpoint rule; the second term of the right-hand side of Eq. (13) is thus approximated by

$$\int_{t^n}^{t^{n+1}} \oint_{\partial D_{i+1/2,j}} (\overrightarrow{f}\,n_x + \overrightarrow{g}\,n_y)\,\mathrm{d}\sigma\,\mathrm{d}t \cong \Delta t \oint_{\partial D_{i+1/2,j}} \left[\overrightarrow{f}(\overrightarrow{U}(x,y,t^{n+1/2}))n_x + \overrightarrow{g}(\overrightarrow{U}(x,y,t^{n+1/2}))n_y\right]\mathrm{d}\sigma. \tag{19}$$

Eq. (19) requires prediction for both $\overrightarrow{U}$ and $\overrightarrow{F}$ at the intermediate time $t^{n+1/2}$, at the cell interfaces. For example we may predict values at the midpoint $a_{i,j}^-$ of the line $a_{i,j}B$, Fig. 4, using an explicit Euler approach and Eq. (11)

$$\overrightarrow{U}_{a_{i,j}B}^{n+1/2} \cong \widetilde{\overrightarrow{U}}_{i,j}(a_{ij}^-, t^n) + \frac{\Delta t}{2}\widetilde{\overrightarrow{U}}_t(a_{ij}^-, t^n) \cong \widetilde{\overrightarrow{U}}_{i,j}(a_{ij}^-, t^n) - \frac{\Delta t}{2}\nabla\cdot\overrightarrow{F}|_{(a_{ij}^-, t^n)}. \tag{20}$$

With the help of the Jacobian matrices, we rewrite Eq. (20) as

$$\overrightarrow{U}_{a_{i,j}B}^{n+1/2} \cong \widetilde{\overrightarrow{U}}_{ij}(a_{i,j}^-, t^n) - \frac{\Delta t}{2h}\left(A\left(\widetilde{\overrightarrow{U}}_{ij}(a_{i,j}^-, t^n)\right)\overrightarrow{U}_{i,x}^{\lim} + B\left(\widetilde{\overrightarrow{U}}_{i,j}(a_{i,j}^-, t^n)\right)\overrightarrow{U}_{i,y}^{\lim}\right). \tag{21}$$
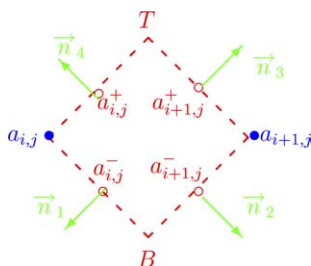
Fig. 4. Diamond cell $D_{i+1/2,j}$ with outward normal vectors.

Using Eqs. (13), (18) and (21), the first step in the x-direction can then be written in the form

$$\overrightarrow{U}_{D_{i+1/2,j}}^{n+1} = \frac{1}{2}\left(\overrightarrow{U}_i^n + \overrightarrow{U}_j^n\right) + \frac{1}{6}\left(\overrightarrow{U}_{i,j;x}^{\lim} - \overrightarrow{U}_{i+1,j;x}^{\lim}\right) - \frac{\Delta t}{h}\left[\left(-\overrightarrow{f}_{a_{i,j}^-}^{n+1/2} - \overrightarrow{g}_{a_{i,j}^-}^{n+1/2}\right).\right.$$
$$\left. + \left(\overrightarrow{f}_{a_{i+1,j}^-}^{n+1/2} - \overrightarrow{g}_{a_{i+1,j}^-}^{n+1/2}\right) + \left(\overrightarrow{f}_{a_{i+1,j}^+}^{n+1/2} + \overrightarrow{g}_{a_{i+1,j}^+}^{n+1/2}\right) + \left(-\overrightarrow{f}_{a_{i,j}^+}^{n+1/2} + \overrightarrow{g}_{a_{i,j}^+}^{n+1/2}\right).\right] \tag{22}$$

4.2. Y-direction

Here we consider two Cartesian cells $C_{i,j}$, $C_{i,j+1}$ such that the line $a_{i,j}a_{i,j+1}$ is parallel to the y-axis. Integrating Eq. (11) on the domain $D_{i,j+1/2} \times [t^n, t^{n+1}]$ and applying Green's theorem defines the value $\overrightarrow{U}_{i,j+1/2}^{n+1}$

$$\mathscr{A}(D_{i,j+1/2})\overrightarrow{U}_{i,j+1/2}^{n+1} = \int\int_{D_{i,j+1/2}} \overrightarrow{U}(x,y,t^n)\,\mathrm{d}A - \int_{t^n}^{t^{n+1}} \oint_{\partial D_{i,j+1/2}} (\overrightarrow{f}\,n_x + \overrightarrow{g}\,n_y)\,\mathrm{d}\sigma\,\mathrm{d}t. \tag{23}$$

Splitting the first integral in the right-hand side of Eq. (23) and using piecewise linear interpolants as for the x-direction gives (see Fig. 5)

$$\int\int_{D_{i,j+1/2}} \overrightarrow{U}(x,y,t^n)\,\mathrm{d}A \approx \frac{h^2}{4}\left(\overrightarrow{U}_{i,j}^n + \overrightarrow{U}_{i,j+1}^n + \frac{1}{3}\overrightarrow{U}_{i,j;y}^{\lim} - \frac{1}{3}\overrightarrow{U}_{i,j+1;y}^{\lim}\right). \tag{24}$$

The flux integral is handled in the same way as in the case of the x-direction. The first time step in the y-direction can thus finally be written in the form
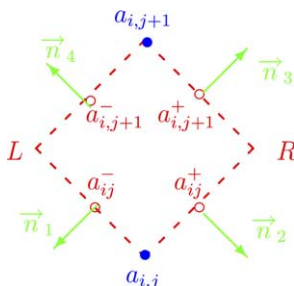

Fig. 5. Dual cell $D_{i,j+1/2}$ with outward normal vectors.

$$\overrightarrow{U}_{D_{i,j+1/2}}^{n+1} = \frac{1}{2}\left(\overrightarrow{U}_{i,j}^{n} + \overrightarrow{U}_{i,j+1}^{n}\right) + \frac{1}{6}\left(\overrightarrow{U}_{i,j;y}^{\lim} - \overrightarrow{U}_{i,j+1;y}^{\lim}\right) - \frac{\Delta t}{h}\left[\left(\overrightarrow{f}_{a_{i,j}^{+}}^{n+1/2} - \overrightarrow{g}_{a_{i,j}^{+}}^{n+1/2}\right)\right.$$
$$\left. + \left(\overrightarrow{f}_{a_{i,j+1}^{+}}^{n+1/2} + \overrightarrow{g}_{a_{i,j+1}^{+}}^{n+1/2}\right) + \left(-\overrightarrow{f}_{a_{i,j+1}^{-}}^{n+1/2} + \overrightarrow{g}_{a_{i,j+1}^{-}}^{n+1/2}\right) + \left(-\overrightarrow{f}_{a_{ij}^{-}}^{n+1/2} - \overrightarrow{g}_{a_{ij}^{-}}^{n+1/2}\right)\right]. \tag{25}$$

4.3. Second time step

For the second time step, we seek an approximation of the solution on the original cell C_i (see Fig. 6.) at time t^{n+2} using as initial data the solution already obtained on dual cells at time t^{n+1}. The computation follows an approach similar to that of the first time step. Integrating Eq. (11) on the domain $C_i \times [t^{n+1}, t^{n+2}]$ and applying Green's theorem yields

$$A(C_i)\overrightarrow{U}_i^{n+2} = \int\int_{C_i} \overrightarrow{U}(x,y,t^{n+1})\,\mathrm{d}A - \int_{t^{n+1}}^{t^{n+2}} \oint_{\partial C_i}(\overrightarrow{f}v_x + \overrightarrow{g}v_y)\,\mathrm{d}\sigma\,\mathrm{d}t. \tag{26}$$

The first integral of the right-hand side of Eq. (26) is decomposed into the contribution of four integrals, and is approximated as

$$\int\int_{C_i} \overrightarrow{U}(x,y,t^{n+1})\,\mathrm{d}A \approx \frac{h^2}{4}\left(\overrightarrow{U}_a^{n+1} + \overrightarrow{U}_b^{n+1} + \overrightarrow{U}_c^{n+1} + \overrightarrow{U}_d^{n+1}\right) + \frac{h^2}{24}\left(\overrightarrow{U}_{a,x}^{\lim} + \overrightarrow{U}_{b,y}^{\lim} - \overrightarrow{U}_{c,x}^{\lim} - \overrightarrow{U}_{d,y}^{\lim}\right). \tag{27}$$

For the flux integral, we proceed as before, using the midpoint rule for the time integration; we need predictions for $\overrightarrow{U}$ and $\overrightarrow{F}$ on the cell interfaces at the intermediate time $t^{n+3/2}$, and we also need the following normal vectors:

$$v_a = (-1,0),\ v_b = (0,-1),\ v_c = (1,0),\ v_d = (0,1).$$

Writing

$$\int_{t^{n+1}}^{t^{n+2}} \oint_{\partial C_i}(\overrightarrow{f}v_x + \overrightarrow{g}v_y)\,\mathrm{d}\sigma\,\mathrm{d}t \cong \Delta t \oint_{\partial C_i}\left[\overrightarrow{f}(\overrightarrow{U}(x,y,t^{n+3/2}))v_x + \overrightarrow{g}(\overrightarrow{U}(x,y,t^{n+3/2}))v_y\right]\mathrm{d}\sigma \tag{28}$$
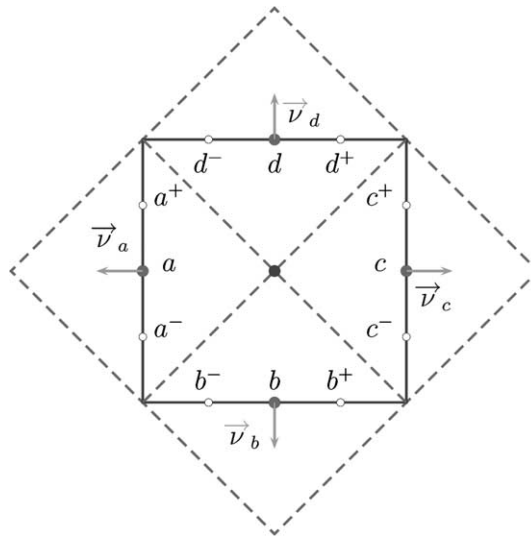

Fig. 6. Original square cell $C_{i,j}$ with its four adjacent oblique dual cells.

we shall approximate the flux on the interface through the point a (Fig. 6) as the arithmetical mean of the fluxes at points a^+ and a^-, $\overrightarrow{F}_a \cong (\overrightarrow{F}(\overrightarrow{U}(a^+)) + \overrightarrow{F}(\overrightarrow{U}(a^-)))/2$. Predictions of the flux on the cell interfaces at the intermediate time may be computed using Eq. (20). The solution at time t^{n+2} takes the following form:

$$\overrightarrow{U}_{i,j}^{n+2} = \frac{1}{4}\left(\overrightarrow{U}_{i-1/2,j}^{n+1} + \overrightarrow{U}_{i+1/2,j}^{n+1} + \overrightarrow{U}_{i,j-1/2}^{n+1} + \overrightarrow{U}_{i,j+1/2}^{n+1}\right) + \frac{1}{24}\left(\overrightarrow{U}_{i-1/2,j;x}^{\lim} + \overrightarrow{U}_{i,j-1/2;y}^{\lim} - \overrightarrow{U}_{i+1/2,j;x}^{\lim} - \overrightarrow{U}_{i,j+1/2;y}^{\lim}\right)$$
$$- \frac{\Delta t}{2h}\left[\left(-\overrightarrow{f}_{a^+}^{n+3/2} - \overrightarrow{f}_{a^-}^{n+3/2}\right) + \left(-\overrightarrow{g}_{b^-}^{n+3/2} - \overrightarrow{g}_{b^+}^{n+3/2}\right) + \left(\overrightarrow{f}_{c^-}^{n+3/2} + \overrightarrow{f}_{c^+}^{n+3/2}\right) + \left(\overrightarrow{g}_{d^+}^{n+3/2} + \overrightarrow{g}_{d^-}^{n+3/2}\right)\right].$$

5. The physical constraint $\nabla \cdot \mathbf{B} = 0$

It is shown in electromagnetic theory that the magnetic field vector $\mathbf{B}$ must be solenoidal, and thus satisfy Maxwell's equation $\nabla \cdot \mathbf{B} = 0$.

If the initial magnetic field satisfies the divergence-free constraint ($\nabla \cdot \mathbf{B}|_{t=0} = 0$), Faraday's law guarantees that it remains divergence-free for all time; indeed, applying the divergence operator to Faraday's law gives:

$$\partial_t \mathbf{B} + \nabla \times (\mathbf{B} \times \mathbf{v}) = 0, \text{(Faraday's law)}$$
$$\Rightarrow \nabla \cdot \partial_t \mathbf{B} + \nabla \cdot \nabla \times (\mathbf{B} \times \mathbf{v}) = 0$$
$$\Rightarrow \partial_t (\nabla \cdot \mathbf{B}) = 0.$$

In a paper published in 1980, Brackbill and Barnes [15] show that non-zero divergence of the magnetic field can lead to non-physical waves and the production of negative pressures and densities in the case of ideal MHD. Several methods have been proposed to satisfy the $\nabla \cdot \mathbf{B} = 0$ constraint: Brackbill and Barnes' *projection method* [15], Powell's *8-wave formulation* method [41], Evans and Hawley's *Constrained Transport* method [21], Tóth's [48] *Central Difference* method and many other methods. In this paper, our approach to enforce the div$\mathbf{B} = 0$ constraint is inspired by Evans and Hawley's constrained transport (CT) method [21]. The different versions of the CT method are nicely presented in [48]; we shall now present the CT method in its original staggered form in a Finite Difference context as described by Tóth [48], before introducing our new approach for Central Finite Volume methods. We present the Constrained Transport approach for a two-dimensional uniform Cartesian grid. The z-component (B_z) of the magnetic field is updated by the base scheme without modification as it does not contribute to $\nabla \cdot \mathbf{B}$. The cell-centered magnetic field is denoted by $\mathbf{B}$ and the magnetic field at the cell interfaces is denoted by $\mathbf{B}$.

Evans and Hawley considered a staggered grid to maintain the divergence-free constraint of the magnetic field at the cell interfaces (see Fig. 7).
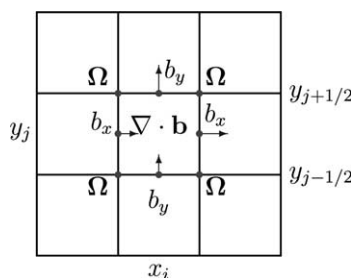

Fig. 7. Staggered magnetic field.

In two space dimensions, the x-component (b_x) of the magnetic field is located at $(x_{i+1/2}, y_j)$ (the cells are being centered at points (x_i, y_j)), and the y-component is located at $(x_i, y_{j+1/2})$.

Let $\Omega = \mathbf{E} \cdot \overrightarrow{k} = -(\mathbf{v} \times \mathbf{B}) \cdot (0, 0, 1)^{\mathrm{T}}$ denote the z-component of the electric field. The main idea of the CT scheme is to place Ω at the cell corners. The induction equation $\partial_t \mathbf{B} + \nabla \times E = 0$ is discretized by simple finite differences along the edges as follows

$$
\begin{aligned}
b_x^{n+1}\big|_{i+1/2,j} &= b_x^n\big|_{i+1/2,j} - \Delta t \frac{\Omega_{i+1/2,j+1/2} - \Omega_{i+1/2,j-1/2}}{\Delta y}, \\
b_y^{n+1}\big|_{i,j+1/2} &= b_y^n\big|_{i,j+1/2} + \Delta t \frac{\Omega_{i+1/2,j+1/2} - \Omega_{i-1/2,j+1/2}}{\Delta x}.
\end{aligned}
\tag{29}
$$

The divergence of **B** is approximated as

$$
\nabla \cdot \mathbf{b}_{i,j} = \frac{b_x\big|_{i+1/2,j} - b_x\big|_{i-1/2,j}}{\Delta x} + \frac{b_y\big|_{i,j+1/2} - b_y\big|_{i,j-1/2}}{\Delta y}.
\tag{30}
$$

Hence, if $\nabla \cdot \mathbf{B}^n = 0$, it is easy to verify that the physical constraint $\nabla \cdot \mathbf{B}^{n+1} = 0$ will be satisfied to the accuracy of round-off errors due to perfect cancelation of terms. The CT idea was combined with Godunov type schemes by Dai and Woodward. Let the superscript *denote the results of the Godunov-type base scheme. For structured grids, spatial and temporal interpolation are used to obtain the cell corner-centered magnetic field as follows:

$$
\bar{\mathbf{B}}_{i+1/2,j+1/2}^{n+1/2} = \frac{1}{8} \left(\mathbf{B}_{i,j}^n + \mathbf{B}_{i+1,j}^n + \mathbf{B}_{i,j+1}^n + \mathbf{B}_{i+1,j+1}^n + \mathbf{B}_{i,j}^* + \mathbf{B}_{i+1,j}^* + \mathbf{B}_{i,j+1}^* + \mathbf{B}_{i+1,j+1}^* \right)
$$

with a similar formula for the velocity field $\mathbf{v}_{i+1/2,j+1/2}^{n+1/2}$. The z-component of the electric field (for ideal MHD) is estimated as

$$
\Omega_{i+1/2,j+1/2}^{n+1/2} = \left(-\bar{\mathbf{v}}_{i+1/2,j+1/2}^{n+1/2} \times \bar{\mathbf{B}}_{i+1/2,j+1/2}^{n+1/2} \right) \cdot \overrightarrow{k}.
$$

Once Ω is obtained we update the **B**-field centered at cell interfaces according to (29) and the components of the cell-centered magnetic field $\mathbf{B}^{n+1}$ are approximated as follows:

$$
\begin{aligned}
B_x^{n+1}\big|_{i,j} &= \frac{b_x^{n+1}\big|_{i+1/2,j} + b_x^{n+1}\big|_{i-1/2,j}}{2}, \\
B_y^{n+1}\big|_{i,j} &= \frac{b_y^{n+1}\big|_{i,j+1/2} + b_y^{n+1}\big|_{i,j-1/2}}{2}.
\end{aligned}
\tag{31}
$$

5.1. Constrained transport for central schemes

Since the numerical schemes we use involve dual staggered cells, the CT approach cannot be applied directly. Here we propose an adaptation of the Constrained Transport approach to maintain the divergence-free property of the magnetic field. Suppose that the solution at time t^n is given on the original Cartesian grid and is such that $\nabla \cdot \mathbf{B}^n = 0$, i.e.,

$$
0 = \nabla \cdot \mathbf{B}^n\big|_{i,j} = \frac{\partial B_x^n}{\partial x}\bigg|_{i,j} + \frac{\partial B_y^n}{\partial y}\bigg|_{i,j} \simeq \frac{B_x^n\big|_{i+1,j} - B_x^n\big|_{i-1,j}}{2\Delta x} + \frac{B_y^n\big|_{i,j+1} - B_y^n\big|_{i,j-1}}{2\Delta y}.
\tag{32}
$$

Performing a first time step, we obtain the solution (at time t^{n+1}) on the dual staggered grid. Let $\mathscr{B}^*$ denote the magnetic field part of this solution on the staggered cells ($D_{i+1/2,j}$-type) in the x-direction. To enforce the $\nabla \cdot \mathscr{B}^{n+1} = 0$ constraint, we first compute the z-component of the electric field ($\Omega = E \cdot k$) as

$$\mathbf{E}_{i+1/2,j}^{n+1/2} = -(\mathbf{v} \times \mathbf{B})_{i+1/2,j}^{n+1/2} = -\frac{1}{2} \left[(\mathbf{v}^{n+1} \times \mathscr{B}^*)_{i+1/2,j} + \frac{(\mathbf{v} \times \mathbf{B})_{i,j}^n + (\mathbf{v} \times \mathbf{B})_{i+1,j}^n}{2} \right]. \tag{33}$$

We then discretize the induction equation using central differences and update the magnetic field at time t^{n+1} as follows:

$$\mathscr{B}_x^{n+1}|_{i+1/2,j} = \frac{B_x^n|_{i,j} + B_x^n|_{i+1,j}}{2} - \Delta t \frac{\Omega_{i+1/2,j+1}^{n+1/2} - \Omega_{i+1/2,j-1}^{n+1/2}}{2\Delta y}, \tag{34}$$

$$\mathscr{B}_y^{n+1}|_{i+1/2,j} = \frac{B_y^n|_{i,j} + B_y^n|_{i+1,j}}{2} + \Delta t \frac{\Omega_{i+3/2,j}^{n+1/2} - \Omega_{i-1/2,j}^{n+1/2}}{2\Delta x}. \tag{35}$$

We shall prove that if $\nabla \cdot \mathbf{B}^n = 0$ on the original grid, the magnetic field $\mathscr{B}$ at time t^{n+1} on the dual cells $D_{i+1/2,j}$ will also satisfy the divergence-free property, i.e.

$$\frac{\mathscr{B}_x^{n+1}|_{i+3/2,j} - \mathscr{B}_x^{n+1}|_{i-1/2,j}}{2\Delta x} + \frac{\mathscr{B}_y^{n+1}|_{i+1/2,j+1} - \mathscr{B}_y^{n+1}|_{i+1/2,j-1}}{2\Delta y} = 0. \tag{36}$$

Using Eqs. (34) and (35) we compute the following quantities:

$$\mathscr{B}_x^{n+1}|_{i+3/2,j} = \frac{B_x^n|_{i+1,j} + B_x^n|_{i+2,j}}{2} - \Delta t \frac{\Omega_{i+3/2,j+1}^{n+1/2} - \Omega_{i+3/2,j-1}^{n+1/2}}{2\Delta y},$$

$$\mathscr{B}_x^{n+1}|_{i-1/2,j} = \frac{B_x^n|_{i-1,j} + B_x^n|_{i,j}}{2} - \Delta t \frac{\Omega_{i-1/2,j+1}^{n+1/2} - \Omega_{i-1/2,j-1}^{n+1/2}}{2\Delta y},$$

$$\mathscr{B}_y^{n+1}|_{i+1/2,j+1} = \frac{B_y^n|_{i,j+1} + B_y^n|_{i+1,j+1}}{2} + \Delta t \frac{\Omega_{i+3/2,j+1}^{n+1/2} - \Omega_{i-1/2,j+1}^{n+1/2}}{2\Delta x},$$

$$\mathscr{B}_y^{n+1}|_{i+1/2,j-1} = \frac{B_y^n|_{i,j-1} + B_y^n|_{i+1,j-1}}{2} + \Delta t \frac{\Omega_{i+3/2,j-1}^{n+1/2} - \Omega_{i-1/2,j-1}^{n+1/2}}{2\Delta x},$$

which we then substitute into Eq. (36); we obtain

$$\nabla \cdot \mathscr{B}^{n+1}|_{i+1/2,j} = \frac{1}{2} (\nabla \cdot \mathbf{B}^n|_{i,j} + \nabla \cdot \mathbf{B}^n|_{i+1,j}) \equiv 0. \tag{37}$$

We update the magnetic field at time t^{n+1} on the $D_{i,j+1/2}$ cells in a similar manner; using the base scheme we perform (with the updated magnetic field components) a second time step to obtain the solution on the original Cartesian grid. Then we update the magnetic field obtained at time t^{n+2} which is also denoted by $\mathbf{B}^*$. The z-component of the electric field is then computed in a way specially designed to satisfy the divergence-free property of the magnetic field, from

$$\begin{aligned}
\mathbf{E}_{i,j}^{n+3/2} &= -(\mathbf{v} \times \mathbf{B})_{i,j}^{n+3/2} \\
&= -\frac{1}{2} \left[(\mathbf{v}^{n+2} \times \mathbf{B}^*)_{i,j} + \frac{1}{4} \left\{ (\mathbf{v} \times \mathbf{B})_{i-1/2,j}^{n+1} + (\mathbf{v} \times \mathbf{B})_{i+1/2,j}^{n+1} + (\mathbf{v} \times \mathbf{B})_{i,j-1/2}^{n+1} + (\mathbf{v} \times \mathbf{B})_{i,j+1/2}^{n+1} \right\} \right].
\end{aligned} \tag{38}$$

We discretize the induction equation on the Cartesian grid

$$B_x^{n+2}|_{i,j} = \frac{1}{4} \left\{ B_x^{n+1}|_{i-1/2,j} + B_x^{n+1}|_{i+1/2,j} + B_x^{n+1}|_{i,j-1/2} + B_x^{n+1}|_{i,j+1/2} \right\} - \Delta t \frac{\Omega_{i,j+1}^{n+3/2} - \Omega_{i,j-1}^{n+3/2}}{2\Delta y}, \tag{39}$$
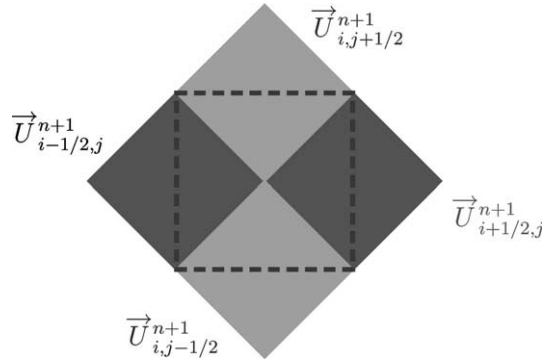
Fig. 8. We use the numerical data given on the original Cartesian cell and those on the four staggered dual cells to approximate the value of the z-component Ω of the electric field at time $t^{n+3/2}$.

$$B_y^{n+2}|_{i,j} = \frac{1}{4}\left\{B_y^{n+1}|_{i-1/2,j} + B_y^{n+1}|_{i+1/2,j} + B_y^{n+1}|_{i,j-1/2} + B_y^{n+1}|_{i,j+1/2}\right\} + \Delta t \frac{\Omega_{i+1,j}^{n+3/2} - \Omega_{i-1,j}^{n+3/2}}{2\Delta x}. \tag{40}$$

As before, we discretize $\nabla \cdot \mathbf{B}_{ij}^{n+2}$ using central differences:

$$\nabla \cdot \mathbf{B}_{jk}^{n+2} \approx \frac{B_x^{n+2}|_{j+1,k} - B_x^{n+2}|_{j-1,k}}{2\Delta x} + \frac{B_y^{n+2}|_{j,k+1} - B_y^{n+2}|_{j,k-1}}{2\Delta y}. \tag{41}$$

We easily prove that the therewith updated magnetic field satisfies the divergence-free constraint (see Fig. 8).

$$\nabla \cdot \mathbf{B}_{ij}^{n+2} = 0 + \frac{1}{4}\left[\nabla \cdot \mathscr{B}_{i-1/2,j}^{n+1} + \nabla \cdot \mathscr{B}_{i+1/2,j}^{n+1} + \nabla \cdot \mathscr{B}_{i,j-1/2}^{n+1} + \nabla \cdot \mathscr{B}_{i,j+1/2}^{n+1}\right] = 0$$

if the physical constraint was satisfied at the previous time.

6. Numerical results

In this section, we present several numerical experiments we have performed for both one and two-dimensional problems.

6.1. One-dimensional test problems

For the first set of numerical tests in one-dimensional space, we have chosen the shock tube problem [44]. We consider the interval $[-1,1]$ of the x-axis, let $\gamma = 5/3$, $B_x = 2$ and consider the initial data for the Riemann problem at $x = 0$, $U_r = [0.989112, -0.013123, 0.026933, 0.010037, 4.024421, 2.002600, 0.971588]$ and $U_l = [1.08, 1.2, 0.01, 0.5, 3.6, 2.0, 0.95]$ with $U = [\rho, u_x, u_y, u_z, B_y, B_z, p]$. This first test case features seven discontinuities. We have considered a grid with 1000 meshpoints. The solution is computed at time $t = 0.25$. We compared our numerical results with those obtained by Ryu and Jones [44]. Figs. 9 and 10 show a very good agreement between the numerical and reference solutions (which were obtained [44] with 10 000 mesh points) when the MC limiter is applied with $\theta = 2$. The agreement is not quite so good when we use the minmod limiter.

Next we have considered a Riemann problem with a compound wave, which consists of a shock and, directly attached, a rarefaction wave [16]; we recall that compound waves cannot arise in solutions of
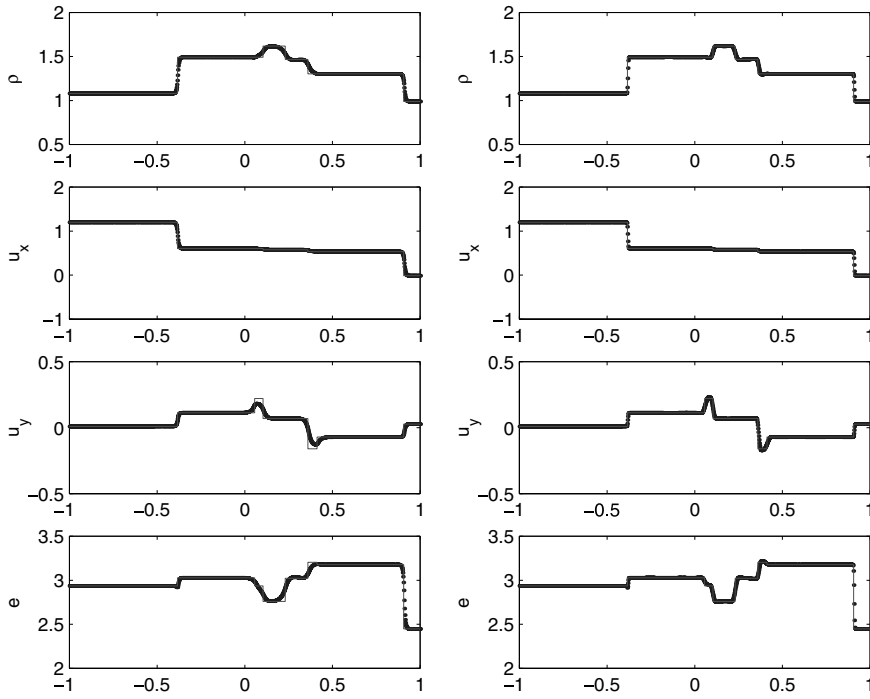
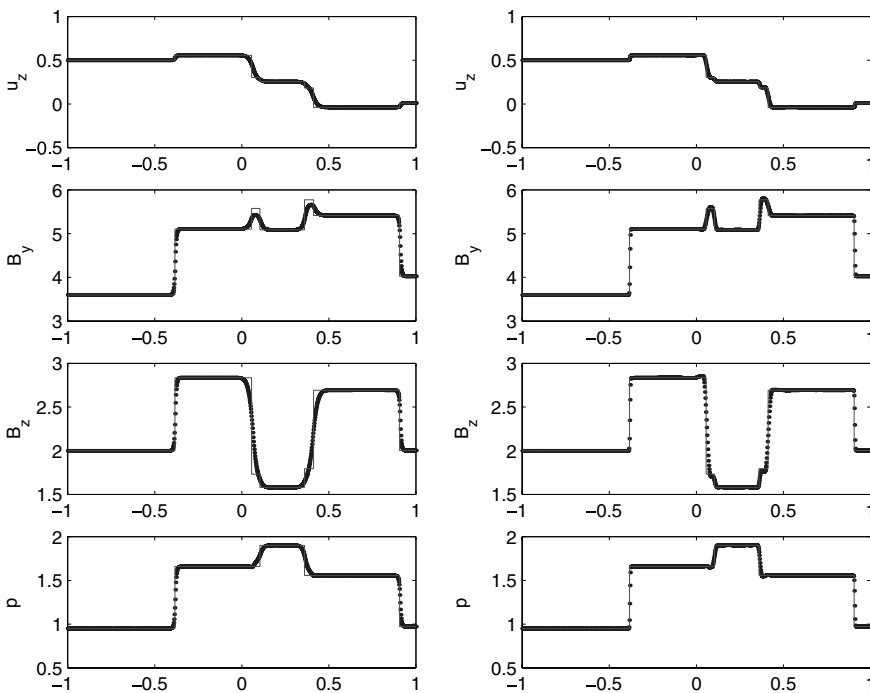Fig. 9. First test case, minmod limiter at left, MC-2 limiter at right.

Fig. 10. First test case (continued), minmod limiter at left, MC-2 limiter at right.

the Euler equations of gas dynamics. We consider the Riemann problem set at $x = 0$ in the interval $[-1,1]$, along with the initial data $U_l = [1,0,0,0,\sqrt{4\pi},0,1]$, $U_r = [0.125,0,0,0,-\sqrt{4\pi},0,0.1]$ and $B_x = 0.75\sqrt{4\pi}$. The solution is computed at time $t = 0.25$ with a CFL condition of 0.485.

We compared our numerical results with those obtained by Brio and Wu [16]. As with the previous test, the agreement with [16] is particularly good when the MC-2 limiter is applied (see Figs. 11 and 12).

Notice that for the above two tests, the reference solutions are available from the following web site: http://www-ian.math.uni-magdeburg.de/anume/testcase/MHD/

6.2. Two-dimensional test problems

We solved a 2D-adaptation of the one-dimensional MHD shock tube problem, involving a compound wave. The computational domain is the rectangle $-1 \leqslant x \leqslant 1, 0 \leqslant y \leqslant 1$. The initial conditions feature a shock along the axis $x = 0$ with the following data: $U_l = [1,0,0,0,\sqrt{4\pi},0,1]$, $U_r = [0.125,0,0,0,-\sqrt{4\pi},0,0.1]$, and $B_x = 0.75\sqrt{4\pi}$. The solution is computed at time $t = 0.25$ with a CFL condition of 0.485. The computations were performed with an MC-$\theta(\theta = 1.5)$ limiter. Fig. 13 shows a very good agreement of the numerical solution (400 data points dotted in blue) with the reference solution of the corresponding one-dimensional problem obtained from 10 000 data points (solid red line), [16].

For our next 2D test, we shall apply our new Constrained transport for central schemes (CTCS) method to satisfy the divergence-free constraint. We consider here the Orszag–Tang MHD turbulence problem, which describes the evolution of a compressible vortex system, which is a complex phenomenon involving the interactions between several shock waves generated during the evolution of the vortex system and traveling at different propagation speeds [48,18]. The initial conditions for our example are: $\rho(x,y) = \rho_0$, $p(x,y) = p_0$, $\mathbf{u}(x,y) = -\sin(2\pi y)\mathbf{i} + \sin(2\pi x)\mathbf{j}$, $\mathbf{B}(x,y) = -\sin(2\pi y)\mathbf{i} + \sin(4\pi x)\mathbf{j}$, with $\rho_0 =$
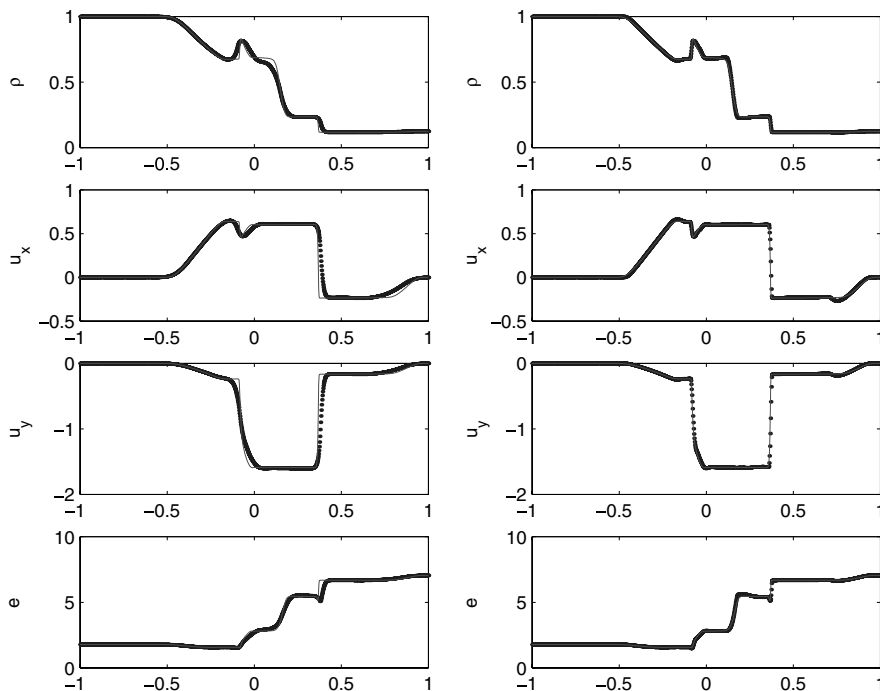

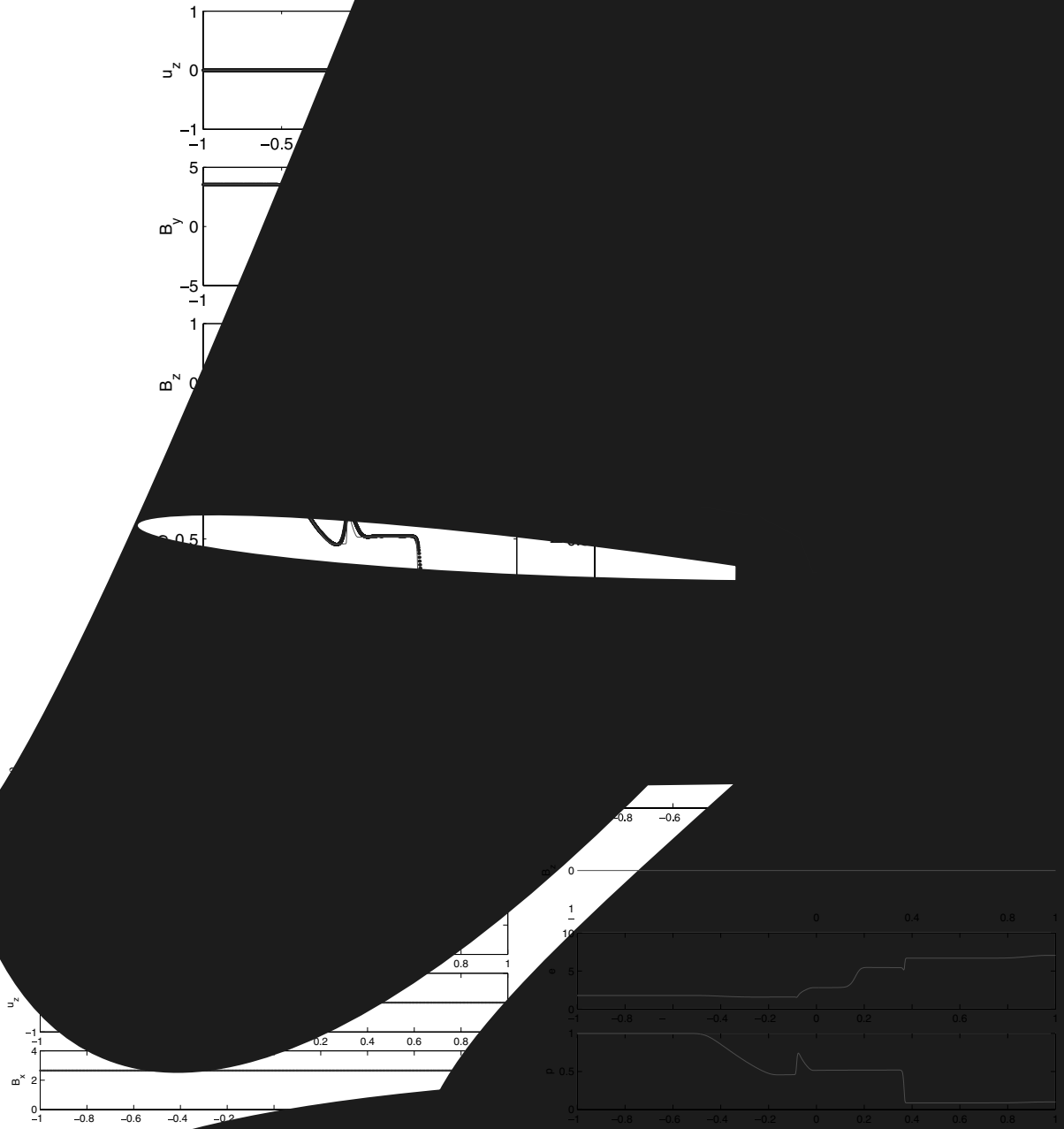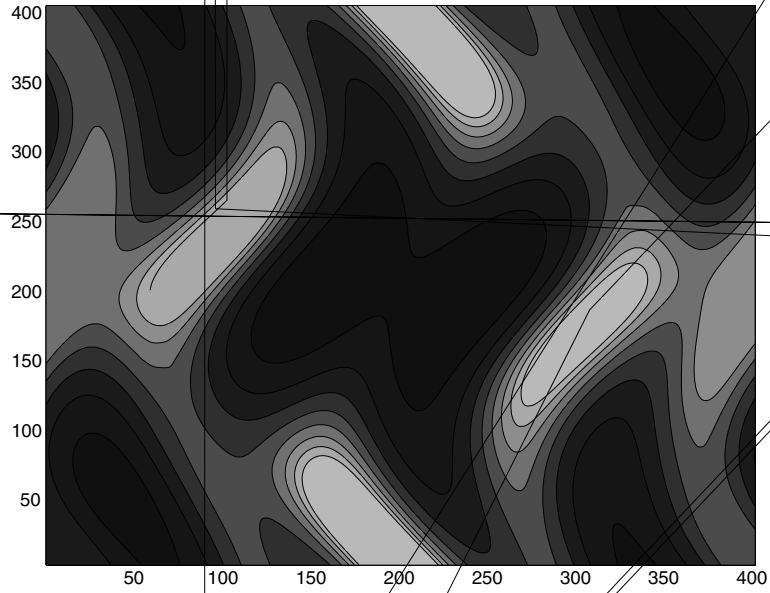Fig. 11. Second test case, minmod limiter at left, MC-2 limiter at right.

Fig. 13. The profile of the solution of the 2D shock tube problem compared with the solution of the one-dimensional corresponding problem.

on the computational domain remain of the order of 10e − 14 throughout the calculations, thus confirming the efficiency of our method.

For the final two-dimensional example we consider a Riemann problem [18], with four initial states for (ρ, p, u_x, u_y) given by $(1, 1, 0.75, 0.5)$ for $x > 0$ and $y > 0$, $(2, 1, 0.75, 0.5)$ for $x < 0$ and $y > 0$, $(1, 1, -0.75, 0.5)$

for $x < 0$ and $y < 0$ and $(3, 1, -0.75, -0.5)$ for $x > 0$ and $y < 0$. We consider a uniform initial magnetic field $\mathbf{B} = (2, 0, 1)$. The solution is computed at time $t = 0.8$ on a 400×400 grid.

Here again we have applied our CTCS method to enforce the divergence-free constraint for the magnetic field, which in this case gave divergence values within a 10e− 14 threshold. Figs. 18 and 19 show the contour lines for the mass density and the magnitude of the magnetic field, respectively.

The contour lines in Fig. 18 are in very good agreement with those appearing in [18].
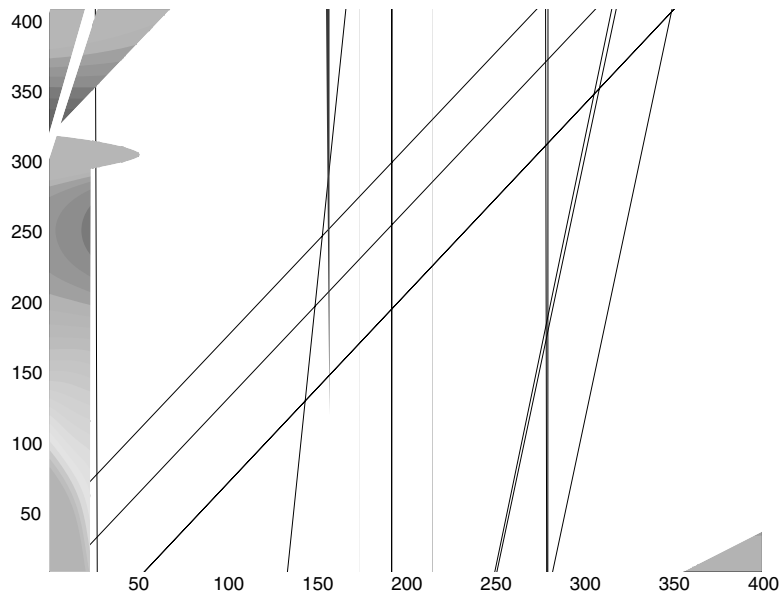
7. Conclusion

In this paper, we have extended our NT-type central finite volume methods to one and two-dimensional problems in MHD, using Cartesian grids for the cells of the original grid, and our previously introduced diamond cells for the dual grid. The fact that the resolution of the Riemann problems at the cell interfaces is by-passed by central schemes has led in all previous numerical experiments performed for scalar conser-

vation equations [2], Euler's equations [3], and Navier–Stokes equations [4], to very substantial computing time reductions. It is therefore anticipated that they will also lead to significant computing time reductions in the case of MHD problems where the solution of the Riemann problems is even more time demanding. This will be illustrated in a forthcoming paper. Inspired from the constrained transport method of Evans and Hawley, we have constructed our CTCS approach to maintain the divergence-free property of the magnetic field for the two-dimensional case. This CTCS method applies indifferently to schemes with Cartesian dual cells or oblique diamond dual cells. A comparison between the CTCS methods for Cartesian and for diamond dual cells will appear in [12] (see Fig. 17).

Our numerical results show the high potential of our base scheme and the CTCS method, which led to divergence values within the range of $10e - 13$, $10e - 14$ for the problems we considered is this paper. It is important to note that the CTCS approach was also applied in the case of staggered schemes such that the dual cells are Cartesian [12]. In our current work, we are applying our method to a few more two-dimensional reference test cases appearing in the literature, as well as several three-dimensional problems.

References

[1] P. Arminjon, M.C. Viallon, Généralisation du schéma de Nessayahu-Tadmor pour une équation hyperbolique à deux dimensions d'espace, CR Acad. Sci. Paris, t.320, serie I, 1995, pp. 85–88.

[2] P. Arminjon, D. Stanescu, M.C. Viallon, A two-dimensional finite volume extension of the Lax–Friedrichs and Nessyahu–Tadmor schemes for compressible flows, in: M. Hafez, K. Oshima, (Eds.), Proceedings of the Sixth International Symposium on Computational Fluid Dynamics, vol. IV, 1995, pp. 7–14.

[3] P. Arminjon, M.C. Viallon, A. Madrane, A finite volume extension of the Lax–Friedrichs and Nessyahu–Tadmor schemes for conservation laws on unstructured grids, revised version with numerical applications, Int. J. Comput. Fluid Dynamics 9 (No. 1) (1997) 1–22.

[4] P. Arminjon, A. Madrane, Staggered mixed finite volume/finite element method for Navier–Stokes equations, AIAA J. 37 (1999) 1558–1571.

[5] P. Arminjon, M.C. Viallon, Convergence of a finite volume extension of the Nessyahu–Tadmor scheme on unstructured grids for a two-dimensional linear hyperbolic equation, SIAM J. Num. Anal. 36 (No. 3) (1999) 738–771.

[6] P. Arminjon, A. Madrane, A. St-Cyr, New Lax–Friedrichs-type finite volume schemes on 2 and 3D Cartesian staggered grids, in: J. Militzer, (Ed.), Seventh Annual Conference of the CFD Society of Canada, 1999, Halifax, 1999, pp. (3-3)–(3-10).

[7] P. Arminjon, A. Madrane, A. St-Cyr, Numerical simulation of 3-D flows with a non-oscillatory central scheme on staggered unstructured tetrahedral grids, in: H. Freistuehler, G. Warnecke, Birkhauser, (Eds.), Proceedings of the Eighth International Conference on Hyperbolic Problems, Int. Series of Num. Math. vol. 140, 2001, pp. 59–68, ISBN 3-7643-6711-3.

[8] P. Arminjon, A. St-Cyr, A. Madrane, New 2 and 3-dimensional non-oscillatory central finite volume methods for staggered Cartesian grids, Appl. Numer. Math. 40/3 (2002) 367–390.

[9] P. Arminjon, A. St-Cyr, Nessyahu–Tadmor-type central finite volume methods without predictor for 3D Cartesian and unstructured tetrahedral grids, Appl. Numer. Math. 46 (2003) 135–155.

[10] P. Arminjon, R. Touma, New three-dimensional structured diamond-staggered finite volume methods, CRM Res. Rep., December 2003.

[11] P. Arminjon, R. Touma, A central diamond-staggered dual cell, finite volume method for ideal magnetohydrodynamics, in: Proceedings of the ICCFD3, International Conference in Computational Fluid Dynamics, Toronto, July 2004.

[12] P. Arminjon, R. Touma, Central schemes with constrained transport divergence treatment for ideal MHD, in: Hyperbolic Problems: Theory, Numerics, Applications, Proceedings of the 10th International Conference on Hyperbolic Problems, Osaka, September 2004.

[13] D.S. Balsara, Total variation diminishing scheme for adiabatic and isothermal magnetohydrodynamics, Astrophys. J. (Suppl.) 116 (1998) 133.

[14] A.A. Barmin, A.G. Kulikovskiy, N.V. Pogorelov, Shock-capturing approach and nonevolutionary solutions in magnetohydrodynamics, J. Comput. Phys. 126 (1996) 77.

[15] J.U. Brackbill, D.C. Barnes, The effect of nonzero $\nabla \cdot \boldsymbol{B}$ on the numerical solution of the magnetohydrodynamic equations, J. Comput. Phys. 35 (1980) 426.

[16] M. Brio, C.C. Wu, An upwind differencing scheme for the equations of ideal magnetohydrodynamics, J. Comput. Phys. 2 (75) (1988) 400–422.

[17] W. Dai, P.R. Woodward, An approximate Riemann solver for ideal magnetohydrodynamics, J. Comput. Phys. 111 (1994) 354–372.

[18] W. Dai, P.R. Woodward, A simple finite difference scheme for multidimensional magnetohydro-dynamical equations, J. Comput. Phys. 142 (1998) 331–369.

[19] W. Dai, P.R. Woodward, Extension of the piecewise parabolic method to multidimensional ideal magnetohydrodynamics, J. Comput. Phys. 115 (1994) 485–513.

[20] A.H. De Sterck, Numerical simulation and analysis of magnetically dominated MHD bow shock ows with applications in space physics, Ph.D. Thesis, Katholieke Unversiteit Leuven, 1999.

[21] C.R. Evans, J.F. Hawley, Simulation of magnetohydrodynamic flows: a constrained transport method, Astrophys. J. 332 (1988) 659.

[22] E. Godlewski, P.-A. Raviart, Numerical Approximation of Hyperbolic Systems of Conservations Laws, Springer, 1996.

[23] S.K. Godunov, A difference scheme for numerical computation of discontinuous solutions of equations of fluid dynamics, Math. Sb. 47 (89) (1959) 271–306.

[24] S.K. Godunov, A. Zabrodine, M. Ivanov, A. Kraïko, G. Prokopov, Résolution numérique des problèmes multidimensionnels de la dynamique des gaz, traduit du russe, Editions Mir, Moscou, 1979.

[25] C. Hirsch, Numerical Computation of Internal and External Flows, vol. I and II, Wiley, New York, 1988-1990.

[26] A. Jameson, Essential elements of computational algorithms for aerodynamic analysis and design, ICASE Report, 97–68, 1997.

[27] A. Jeffrey, T. Taniuti, Non-linear Wave Propagation, Academic Press, New York, 1964.

[28] G. Jiang, E. Tadmor, Non-oscillatory central schemes for multidimensional hyperbolic conservation laws, SIAM J. Sci. Comput. 19 (1998) 1892–1917.

[29] G. Jiang, C.C. Wu, A high-order WENO finite difference scheme for the equations of ideal magnetohydrodynamics, J. Comput. Phys. 150 (1999) 561–594.

[30] T. Katsaounis, D. Levy, A modified structured central scheme for 2D hyperbolic conservation laws, Appl. Math. Lett. 12 (6) (1999) 86–89.

[31] D. Kröner, Numerical Schemes for Conservation Laws, in Wiley–Teubner Series, Adv. Numer. Math., Wiley, Stuttgart, 1997.

[32] L.D. Landau, E. Lifshitz, Electrodynamics of Continuous Media, Pergamon, New York, 1960.

[33] P.D. Lax, Weak solutions of nonlinear hyperbolic equation and their numerical computation, Comm. Pure Appl. Math. 7 (1954) 159–193.

[34] P.D. Lax, B. Wendroff, Systems of conservation laws, Comm. Pure Appl. Math. 13 (1960) 217–237.

[35] R. Leveque, Finite Volume Methods for Hyperbolic Problems, Cambridge University Press, 2002.

[36] K.-A. Lie, S. Noelle, Remarks on high-resolution non-oscillatory central schemes for multidimensional systems of conservation laws. Part I: An improved quadrature rule for the flux computation, Preprint No. 679, Sonderforschungsbereich 256, Rheinische Friedrich-Wilhelms-Universitaet, Bonn, Germany, 2000.

[37] H. Nessyahu, E. Tadmor, Non-oscillatory central differencing for hyperbolic conservation laws, J. Comput. Phys. 87 (2) (1990) 408–463.

[38] L. Pareschi, G. Puppo, G. Russo, Central Runge–Kutta schemes for Conservation Laws, Preprint submitted to SIAM J. Sci. Comput., 2003.

[39] K.G. Powell, P.L. Roe, T.J. Linde, T.I. Gombosi, D.L. De Zeeuw, A solution-adaptive upwind scheme for ideal magnetohydrodynamics, J. Comput. Phys. 154 (1999) 284.

[40] K.G. Powell, P.L. Roe, R.S. Myong, T. Gombosi, D. De Zeeuw, An upwind scheme for magnetohy-drodynamics, AIAA Paper 95-1704-CP, 1995.

[41] K.G. Powell, An Approximate Riemann Solver for MHD, ICASE NASA, Langley Research Center, Contract Rep. 194902, ICASE Rep. 94–25, Hampton, VA, 1994.

[42] R.D. Richtmyer, K.W. Morton, Difference Methods for Initial-value Problems, Interscience, New York, 1967.

[43] G. Russo, in: I. Struckmeier, (Eds.), Central schemes and Systems of Balance Laws, Hyp. Part. Diff. Eq., Theo., Num. App., A. Meister, Vieweg, Wiesbaden (D), 2002.

[44] D. Ryu, T.W. Jones, Numerical magnetohydrodynamics in astrophysics: algorithm and tests for one-dimensional flow, Astrophys. J. 442 (1995) 228.

[45] C.W. Schulz-Rinne, J.P. Collins, H.M. Glaz, Numerical solution of the Riemann problem for two-dimensional gas dynamics, SIAM J. Sci. Comput. 14 (1993) 1394–1414.

[46] D. Serre, in: D. Diderot, (Ed.), Systèmes de lois de conservation, Paris, vols. I and II, 1996.

[47] G.A. Sod, Numerical Methods in Fluid Dynamics, Cambridge University Press, 1985.

[48] G. Tóth, The $\nabla \cdot \mathbf{B} = 0$ constraint in shock-capturing magnetohydrodynamics codes, J. Comput. Phys. 161 (2000) 605–652.

[49] G. Tóth, D. Odstrčil, Comparison of some flux corrected transport and total variation diminishing numerical schemes for hydrodynamic and magnetohydrodynamic problems, J. Comput. Phys. 128 (1996) 82.

[50] B. van Leer, Towards the ultimate conservative difference scheme IV. A new approach to numerical convection, J. Comput. Phys. 23 (1977) 276–299.

[51] B. van Leer, Towards the ultimate conservative difference scheme V. A second-order sequel to Godunov's method, J. Comput. Phys. 32 (1979) 101–136.

[52] A.L. Zachary, P. Colella, A high-order Godunov method for the equations of ideal magnetohydrodynamics, J. Comput. Phys. 99 (1992) 341–347.

[53] A.L. Zachary, A. Malagoli, P. Colella, A higher-order Godunov method for multi-dimensional ideal magnetohydrodynamics, SIAM J. Sci. Comput. 15 (1994) 263–284.